JPE 17-3-10

https://doi.org/10.6113/JPE.2017.17.3.674
ISSN(Print): 1598-2092 / ISSN(Online): 2093-4718

An Improved Model Predictive Direct Torque Control for Induction Machine Drives

Wenxiang Song[†], Shengkang Le[*], Xiaoxin Wu[*], and Yi Ruan[*]

[†,*]School of Mechatronic Engineering and Automation, Shanghai University, Shanghai, China

Abstract

The conventional model predictive direct torque control (MPDTC) method uses all of the voltage vectors available from a two level voltage source inverter for the prediction of the stator flux and stator current, which leads to a heavy computational burden. This paper proposes an improved model predictive direct torque control method. The stator flux predictive controller is obtained from an analysis of the relationship between the stator flux and the torque, which can be used to calculate the desired voltage vector based on the stator flux and torque reference. Then this method only needs to evaluate three voltage vectors in the sector of the desired voltage vector. As a result, the computational burden of the conventional MPDTC is effectively reduced. The time delay introduced by the computational time causes the stator current to oscillate around its reference. It also increases the current and torque ripples. To address this problem, a delay compensation method is adopted in this paper. Furthermore, the switching frequency of the inverter is significantly reduced by introducing the constraint of the power semiconductor switching number to the cost function of the MPDTC. Both simulation and experimental results are presented to verify the validity and feasibility of the proposed method.

Key words: Delay compensation, Direct torque control, Induction machine, Model predictive control

I. INTRODUCTION

Field-Oriented Control (FOC) [1] and Direct Torque Control (DTC) [2]-[5] are widely used in high-performance ac drive application. The main difference between these control strategies is that the torque and flux are directly controlled using torque and flux hysteresis comparators in DTC, whereas the d-axis and q-axis components of the stator current are used to control the torque and flux in the FOC. Therefore, the dynamic performance of the DTC control method is better than that of the FOC control method. However, DTC has some drawbacks such as high torque and flux ripples and a variable switching frequency in the power semiconductors [6], [7]. A novel switching table, which can effectively reduce the torque ripple of permanent magnet synchronous motors, has been presented in [8]. The root cause of the variable switching frequency in DTC is the use of hysteresis controllers [9]. To overcome this problem, various methods have been proposed in the literature including the use of a new torque and flux controllers [6] and fuzzy logic control techniques [10].

In the late 1970s, Model Predictive Control (MPC) was applied as a control algorithm in the chemical process industry. MPC is a nonlinear predictive control strategy with a strong ability to handle nonlinear constraints. It is also a flexible control strategy due to its use of a cost function as the optimization criterion [11]. Although MPC is widely used in the chemical process industry, it still has disadvantages such as the high requirements of the controller performance due to the need for online calculations [12]. Due to the limitation of microprocessors calculation ability, model predictive control has rarely been applied in the electrical drive field over the last few decades [13]. Nowadays, the development of digital signal processors has made it possible to use MPC in the electrical drives field. In [14], a MPC method was applied in the power electronics field for the first time. In fact, the conventional DTC is also widely interpreted as a predictive control strategy. However, the conventional DTC can only roughly predict the switching state in the next sampling period due to its lack of an explicit prediction model and optimization criterion.

To improve the torque performance of the conventional

Manuscript received Jul. 18, 2016; accepted Feb. 15, 2017
Recommended for publication by Associate Editor Gaolin Wang.
[†]Corresponding Author: wxsong@shu.edu.cn
Tel: +86-138-1849-9089, Shanghai University
[*]School of Mechatronic Eng. & Automat., Shanghai University, China

DTC, the optimal voltage vector is selected by using a finite-control-set model predictive torque control strategy with a deadbeat solution [15]. Finite-control-set model predictive torque control is a control strategy that utilizes a system discrete time model to predict the future state of the system, and instead of modulator, and utilizes a cost function to obtain the optimal switching state [16]-[18]. Model Predictive DTC (MPDTC) is quite different from the conventional DTC. MPDTC uses a cost function to select the optimal voltage vector so that it can improve the performance in solving nonlinear constraints, such as switching frequency, switching loss, etc. For the current control of a voltage source inverter with a resistance and inductance load, the predictive current control method is presented in [19]. It uses a discrete-time model of the system to predict the future value of the load current for all of the possible voltage vectors, and the optimal voltage vector is selected using a quality function. Based on the finite-control-set model predictive control, a torque predictive control method was proposed in [20]. The optimal switching state and switching time point are obtained by predicting the values of the torque and flux in the next sampling period and by using torque ripples as a cost function. Although the torque ripples are reduced, this method has some drawbacks such as a high switching frequency.

The conventional MPDTC method is improved in this paper. The desired voltage vector is calculated by the use of a stator flux predictive controller. Accordingly, the sector of the desired voltage vector can be determined. In the end, the three voltage vectors in this sector, which will be evaluated by the cost function, are obtained. In terms of the effect of the time delay, it is compensated to improve the performance of the system. In addition, this paper presents a Low Switching Frequency Model Predictive DTC (LSFMPDTC) method to reduce the switching frequency of the inverter by introducing the constraint of the power semiconductors switching number to the cost function.

This paper is organized as follows. Section II presents mathematical models of the tested induction machine. Section III introduces the conventional MPDTC method. Section IV explains the improved MPDTC method. Simulation and experimental results are given in Section V and Section VI, and the conclusion of the paper is in the last section.

II. Mathematical Model of an Induction Machine

The dynamic equations of an IM with stator the flux $\boldsymbol{\psi}_s$ and stator current $\boldsymbol{i}_s$ as state variables can be expressed in the stationary $\alpha\beta$ frame as:

$$\frac{d\psi_{s\alpha}}{dt} = -R_s i_{s\alpha} + u_{s\alpha} \tag{1}$$

$$\frac{d\psi_{s\beta}}{dt} = -R_s i_{s\beta} + u_{s\beta} \tag{2}$$

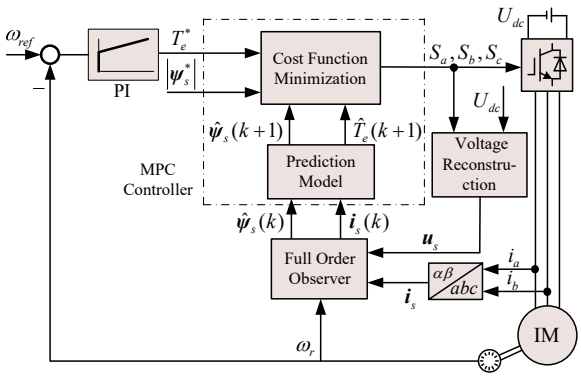

Fig. 1. Block diagram of the conventional MPDTC.

$$\frac{di_{s\alpha}}{dt} = \frac{R_r}{\delta}\psi_{s\alpha} + \frac{L_r\omega_r}{\delta}\psi_{s\beta} - \frac{R_s L_r + R_r L_s}{\delta} i_{s\alpha} - \omega_r i_{s\beta} + \frac{L_r}{\delta} u_{s\alpha} \tag{3}$$

$$\frac{di_{s\beta}}{dt} = \frac{R_r}{\delta}\psi_{s\beta} - \frac{L_r\omega_r}{\delta}\psi_{s\alpha} - \frac{R_s L_r + R_r L_s}{\delta} i_{s\beta} + \omega_r i_{s\alpha} + \frac{L_r}{\delta} u_{s\beta} \tag{4}$$

where $\psi_{s\alpha}$, $\psi_{s\beta}$ and $i_{s\alpha}$, $i_{s\beta}$ are the $\alpha\beta$ frame components of the stator flux and stator current, respectively, $u_{s\alpha}$, $u_{s\beta}$ are the $\alpha\beta$ frame components of the stator voltage, and $\delta = L_s L_r - L_m^2$.

R_s: stator resistance
R_r: rotor resistance
L_s: stator inductance
L_r: rotor inductance
L_m: mutual inductance
ω_r: electrical rotor speed

The magnitude of the stator flux can be represented as:

$$|\boldsymbol{\psi}_s| = \sqrt{\psi_{s\alpha}^2 + \psi_{s\beta}^2} \tag{5}$$

The electromagnetic torque T_e is given by:

$$T_e = \frac{3}{2} n_p \boldsymbol{\psi}_s \otimes \boldsymbol{i}_s \tag{6}$$

where n_p is the number of pole pairs and $\otimes$ represents the cross-product.

III. Conventional Model Predictive Direct Torque Control

A. Structure of the Control System

A diagram of the conventional MPDTC is shown in Fig. 1. Compared to the conventional DTC, the outer loop of the conventional MPDTC is also a speed loop, and the reference of torque is obtained from a PI regulator. The main difference between the two control methods is that the inner loop of the conventional MPDTC employs a model predictive controller instead of the stator flux and torque hysteresis comparators used in the conventional DTC. The model predictive controller is constituted by the prediction models of the torque and stator flux and the cost function, while the predictive values of the stator flux and torque are obtained using the prediction models. Finally, the voltage vector that minimizes the cost function will be selected and applied to

the inverter.

B. Full Order Observer

The performance of the MPDTC is highly dependent on the accuracy of the flux observer. Thus, to improve the accuracy of the flux observer, a full order observer is adopted in this paper. Mathematical models of the full order observer are expressed as:

$$\begin{cases} \dfrac{d\hat{\boldsymbol{i}}_s}{dt} = (-\dfrac{R_s L_r + R_r L_s}{\delta} + j\omega_r)\hat{\boldsymbol{i}}_s + \dfrac{R_r - jL_r\omega_r}{\delta}\hat{\boldsymbol{\psi}}_s \\ \qquad + \dfrac{L_r}{\delta}\boldsymbol{u}_s + g_1(\boldsymbol{i}_s - \hat{\boldsymbol{i}}_s) \\ \dfrac{d\hat{\boldsymbol{\psi}}_s}{dt} = -R_s\hat{\boldsymbol{i}}_s + \boldsymbol{u}_s + g_2(\boldsymbol{i}_s - \hat{\boldsymbol{i}}_s) \end{cases} \tag{7}$$

where $\hat{\boldsymbol{i}}_s$, $\hat{\boldsymbol{\psi}}_s$ are the estimated values of the stator current and stator flux, respectively, and g_1, g_2 are the feedback coefficients of the current error, which can be expressed as follows:

$$\begin{cases} g_1 = 2b \\ g_2 = \dfrac{\delta b}{L_m} \end{cases} \tag{8}$$

where b is a negative constant gain [21]. The gain matrix of Equ. (8) is characterized by the fact that the poles of the observer are shifted to the left when compared with the poles of the induction machine, the imaginary part is small at a high speed, and the error convergence rate is improved.

C. Prediction Model

The forward Euler approximation can be described as follows:

$$\frac{dx}{dt} \approx \frac{x(k+1) - x(k)}{T_s} \tag{9}$$

where T_s is the sampling period.

To predict the values of the stator current and stator flux in the next sampling instant, the forward Euler approximation expressed in Equ. (9) is employed to discretize Eqns. (1)-(4). The prediction models of the stator current and stator flux are expressed as follows:

$$\psi_{s\alpha}(k+1) = \psi_{s\alpha}(k) - R_s T_s i_{s\alpha}(k) + T_s u_{s\alpha}(k) \tag{10}$$

$$\psi_{s\beta}(k+1) = \psi_{s\beta}(k) - R_s T_s i_{s\beta}(k) + T_s u_{s\beta}(k) \tag{11}$$

$$\begin{aligned} i_{s\alpha}(k+1) = {} & \frac{R_r T_s}{\delta}\psi_{s\alpha}(k) + \frac{L_r\omega_r T_s}{\delta}\psi_{s\beta}(k) + \\ & (1 - \frac{R_s L_r + R_r L_s}{\delta}T_s)i_{s\alpha}(k) - \omega_r T_s i_{s\beta}(k) + \frac{L_r T_s}{\delta}u_{s\alpha}(k) \end{aligned} \tag{12}$$

$$\begin{aligned} i_{s\beta}(k+1) = {} & \frac{R_r T_s}{\delta}\psi_{s\beta}(k) - \frac{L_r\omega_r T_s}{\delta}\psi_{s\alpha}(k) + \\ & (1 - \frac{R_s L_r + R_r L_s}{\delta}T_s)i_{s\beta}(k) + \omega_r T_s i_{s\alpha}(k) + \frac{L_r T_s}{\delta}u_{s\beta}(k) \end{aligned} \tag{13}$$

Substituting (10) and (11) into (5), the predictive value of the stator flux magnitude $|\psi_s|$ is represented as:

$$|\boldsymbol{\psi}_s(k+1)| = \sqrt{\psi_{s\alpha}^2(k+1) + \psi_{s\beta}^2(k+1)} \tag{14}$$

Substituting (10), (11), (12) and (13) into (6), the predictive value of the torque T_e is represented as:

$$T_e(k+1) = \frac{3}{2}n_p\boldsymbol{\psi}_s(k+1) \otimes \boldsymbol{i}_s(k+1) \tag{15}$$

For a two level voltage source inverter, there are eight discrete voltage vectors available, $\boldsymbol{u}_0$, $\boldsymbol{u}_1$, …, $\boldsymbol{u}_7$, if only one voltage vector is applied during the whole sampling period. The predictive values of the stator flux magnitude $|\psi_{si}^p(k+1)|$ and torque $T_{ei}^p(k+1)$ are obtained using Eqns. (14) and (15), when the ith voltage vector is applied to the inverter.

D. Cost Function Optimization

The cost function of the model predictive control is flexible and multifarious. In DTC, the aim is to force both the stator flux and the torque to quickly track their own reference values [13]. Therefore, the relative errors of the torque and flux can be regard as a cost function of MPDTC:

$$\begin{aligned} & min.\ J = k_\psi \frac{|\boldsymbol{\psi}_s^* - \boldsymbol{\psi}_s^p(k+1)|}{\boldsymbol{\psi}_{sN}} + k_T \frac{|T_e^* - T_e^p(k+1)|}{T_{eN}} \\ & s.t.\ \ \boldsymbol{u}_s(k) \in \{\boldsymbol{u}_0, \boldsymbol{u}_1, \ldots, \boldsymbol{u}_6, \boldsymbol{u}_7\} \end{aligned} \tag{16}$$

where ψ_s^* and T_e^* are the reference values of the stator flux and torque, ψ_{sN} and T_{eN} are the rated values of the stator flux and torque, and k_ψ and k_T are the weighting factors of the stator flux and torque. The control of the stator flux and torque can be achieved flexibly by selecting suitable values for k_ψ and k_T. For the eight voltage vectors, the respective values J of the cost function are calculated using (16), and the voltage vector which minimizes the cost function (16) is the optimal voltage vector.

By using Equ. (16) as a cost function, the stator flux and torque can track their reference values quickly. However, the average switching frequency of the inverter is higher than what the conventional DTC. In the medium-voltage electrical drives field, the aim is to develop a control algorithm that achieves the same performance as the conventional DTC, while reducing the average switching frequency of the inverter. Therefore, by adding the constraint of the power semiconductors switching number to the cost function, the cost function of the LSFMPDTC can be expressed as:

$$\begin{aligned} & min.\ J = k_\psi \frac{|\boldsymbol{\psi}_s^* - \boldsymbol{\psi}_s^p(k+1)|}{\boldsymbol{\psi}_{sN}} + k_T \frac{|T_e^* - T_e^p(k+1)|}{T_{eN}} \\ & \qquad + k_f \sum_{x=a,b,c} |S_x(k) - S_x(k-1)| \\ & s.t.\ \ \boldsymbol{u}_s(k) \in \{\boldsymbol{u}_0, \boldsymbol{u}_1, \ldots, \boldsymbol{u}_6, \boldsymbol{u}_7\} \end{aligned} \tag{17}$$

where $S_x(k)$ is the current switching state, $S_x(k\text{-}1)$ is the last switching state, and k_f is the weighting factor of the power semiconductors switching number. The average switching frequency of the inverter can be reduced effectively by increasing the value of k_f. However, the increase of k_f to reduce the average switching frequency of the inverter should

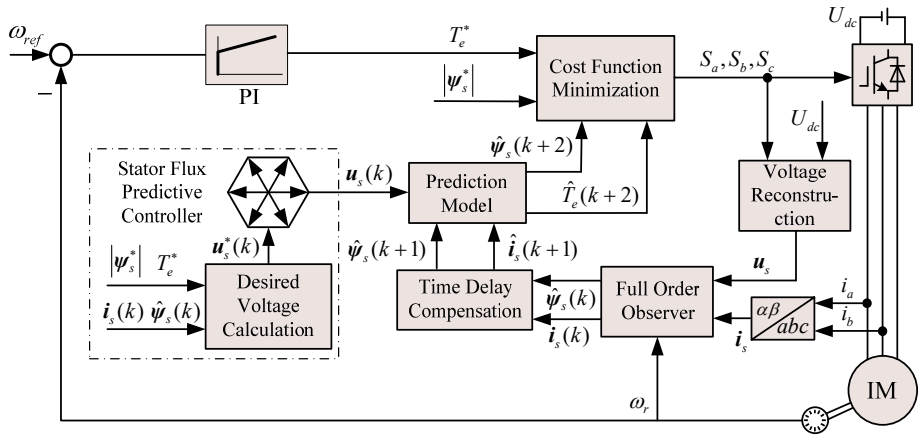

Fig. 2. Block diagram of the improved MPDTC.

be appropriate, or the motor may go out of control.

A comparison of Eqns. (16) and (17) shows that, the MPDTC method utilizes the minimum deviation of the torque and flux as the optimization criterion to select the optimal voltage vector. When changing the voltage vector, it does not need to consider the influence on the switching frequency. However, the LSFMPDTC method should take that condition into account. For example, if a voltage vector has the minimum torque and flux deviation, but produces a high switching frequency, then this voltage vector will not be regarded as the optimal voltage vector. This means that the torque and flux deviations generated by the optimal voltage vector of the LSFMPDTC may not be the minimum. In this situation, a voltage vector is applied to the inverter continuously for several control periods. As a result, the switching frequency can be reduced. In addition, increasing the weight factor k_f makes this phenomenon appear more frequently.

IV. Improved Model Predictive Direct Torque Control

A diagram of the improved MPDTC system is illustrated in Fig. 2. Compared with the conventional MPDTC, the stator flux predictive controller and time delay compensation are introduced in the improved MPDTC to improve the control performance. Detailed information about the stator flux predictive controller and time delay compensation will be described in the following sections.

A. Stator Flux Predictive Controller

Due to the eight voltage vectors in a two level voltage source inverter, the conventional MPDTC method needs to evaluate all eight voltage vectors in the process of selecting the best voltage vector. Thus, the computational burden is significantly increased. In this paper, a stator flux predictive controller is designed to reduce the computational burden of the conventional MPDTC. By using the stator flux predictive controller, the desired voltage vector is calculated based on the torque and stator flux reference. Then, the improved MPDTC only needs to evaluate the three voltage vectors in the sector of the desired voltage vector. Hence, the computational burden is effectively reduced. In the following, the design process of the stator flux controller is described in detail.

The electromagnetic torque can be expressed as:

$$\begin{aligned} T_e &= \frac{3}{2} n_p \frac{L_m}{\delta} \boldsymbol{\psi}_r \otimes \boldsymbol{\psi}_s \\ &= \frac{3}{2} n_p \frac{L_m}{\delta} |\boldsymbol{\psi}_r| |\boldsymbol{\psi}_s| \sin(\angle \boldsymbol{\psi}_s - \angle \boldsymbol{\psi}_r) \end{aligned} \tag{18}$$

From Equ. (18), the relationship between the stator flux angle and the rotor flux angle can be obtained as:

$$\angle \boldsymbol{\psi}_s = \angle \boldsymbol{\psi}_r + \sin^{-1}\left(\frac{2\delta T_e}{3 n_p L_m |\boldsymbol{\psi}_r| |\boldsymbol{\psi}_s|}\right) \tag{19}$$

Substituting the torque reference value T_e^* and stator flux amplitude reference value $|\psi_s^*|$ into (19), the reference value of the stator flux angle can be expressed as:

$$\angle \boldsymbol{\psi}_s^* = \angle \boldsymbol{\psi}_r + \sin^{-1}\left(\frac{2\delta T_e^*}{3 n_p L_m |\boldsymbol{\psi}_r| |\boldsymbol{\psi}_s^*|}\right) \tag{20}$$

Therefore, by using the torque reference value T_e^* and stator flux amplitude reference value $|\boldsymbol{\psi}_s^*|$, the $\alpha\beta$ frame components of the stator flux reference value $\boldsymbol{\psi}_s^*$ can be obtained as:

$$\begin{cases} \psi_{s\alpha}^* = |\boldsymbol{\psi}_s^*| \cos \angle \boldsymbol{\psi}_s^* \\ \psi_{s\beta}^* = |\boldsymbol{\psi}_s^*| \sin \angle \boldsymbol{\psi}_s^* \end{cases} \tag{21}$$

From Eqns. (10) and (11), if $\psi_{s\alpha}(k+1)=\psi_{s\alpha}^*$ and $\psi_{s\beta}(k+1)=\psi_{s\beta}^*$, the $\alpha\beta$ frame components of the desired voltage vector $\boldsymbol{u}_s^*$ can be obtained as:

$$\begin{cases} u_{s\alpha}^* = \dfrac{\psi_{s\alpha}^* - \psi_{s\alpha}(k)}{T_s} + R_s i_{s\alpha}(k) \\ u_{s\beta}^* = \dfrac{\psi_{s\beta}^* - \psi_{s\beta}(k)}{T_s} + R_s i_{s\beta}(k) \end{cases} \tag{22}$$

The desired voltage vector $\boldsymbol{u}_s^*$ can be obtained from (22), and is adopted for the stator flux predictive control. Then, the sector of the desired voltage vector $\boldsymbol{u}_s^*$ is calculated, and the three voltage vectors in this sector are obtained. Finally, the three voltage vectors are evaluated by the cost function, and the voltage vector that minimizes the cost function is the optimal voltage vector. For example, if the desired voltage vector $\boldsymbol{u}_s^*$ is in sector I, then the three voltage vectors are $\boldsymbol{u}_0$(000/111), $\boldsymbol{u}_1$(100) and $\boldsymbol{u}_2$(110), respectively. Considering that the inverter has two zero vectors, the zero vector is selected based on the criterion of the minimum switching number between different voltage vectors. For example, if the optimal voltage vector of the previous period is $\boldsymbol{u}_1$(100), then the voltage vector $\boldsymbol{u}_0$(000) will be selected for the optimization solution.

B. Time Delay Compensation

Fig. 3 gives a schematic diagram of the model predictive control in which the solid lines are the actual trajectory given by the application of the optimal voltage vector, and the dashed lines represent the predictions for $i_{s\alpha}$. This simplified schematic diagram offers current trajectories of three voltage vectors. The current predictive control under ideal conditions is shown in Fig. 3(a). In this case, the calculating time is negligible. This means that if the optimal voltage vector $u_{opt}(k)$ is calculated at the time t_k, the value of $u_{opt}(k)$ will be applied to the inverter instantly. However, in practical applications, due to the limitations in terms of microprocessors calculation ability, the calculation time is considerable. Therefore, the optimal voltage vector calculated at the time t_k is applied to the inverter at t_{k+1} and the measured stator current $\boldsymbol{i}_s(k)$ and stator flux $\boldsymbol{\psi}_s(k)$ are already changed into $\boldsymbol{i}_s(k+1)$ and $\boldsymbol{\psi}_s(k+1)$ at the k+1th sampling instant. This introduces a considerable time delay into the system. As a consequence, the stator current oscillates around its reference, and the current and torque ripples increase. The results are shown in Fig. 3(b).

To compensate this time delay, a two-step prediction of the stator current and flux is adopted. First, the optimal voltage vector $u_{opt}(k+1)$ needed for the time t_{k+1} is calculated at t_k. Then $u_{opt}(k+1)$ is applied to the inverter at t_{k+1}, as shown in Fig. 3(c). By comparing Fig. 3(b) with Fig. 3(c), it can be seen that the time delay increases the current ripple, which leads to the same voltage vector being continuously applied to the inverter for several control periods. As a result, the switching frequency of the MPDTC without delay compensation is lower than that of the MPDTC with delay compensation. The switching frequency comparison results of these two methods are given in the following section.

By using the stator current $\boldsymbol{i}_s(k+1)$ and stator flux $\boldsymbol{\psi}_s(k+1)$ as starting conditions for the prediction of the stator current and stator flux, the predictive values of the stator current $\boldsymbol{i}_s(k+2)$ and stator flux $\boldsymbol{\psi}_s(k+2)$ at the k+2th sampling instant can be expressed as:

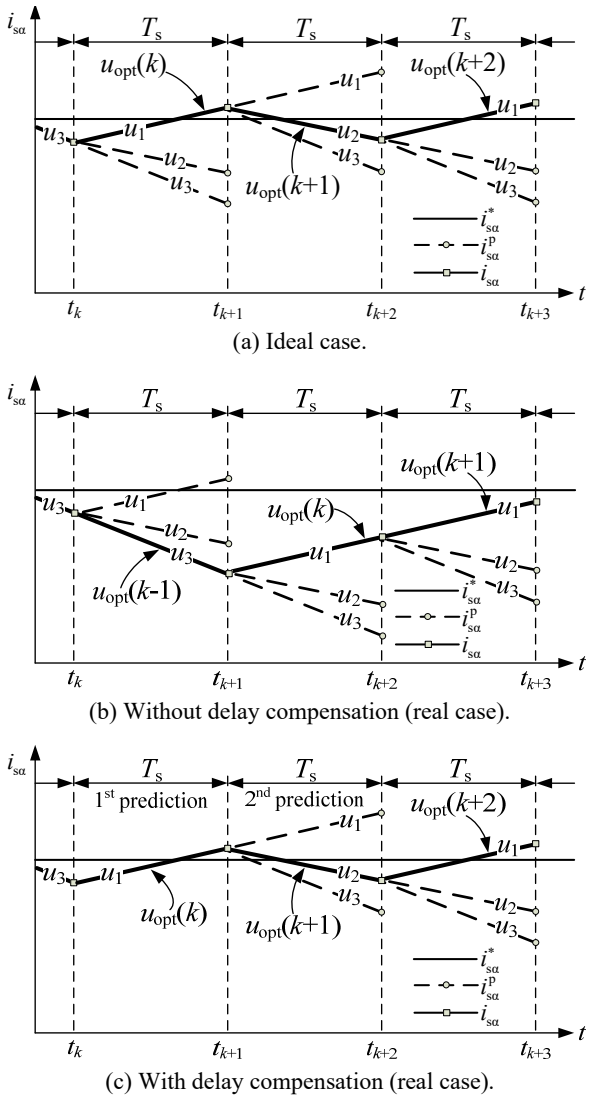

Fig. 3. Schematic diagrams of the model predictive control.

$$\psi_{s\alpha}(k+2)=\psi_{s\alpha}(k+1)-R_sT_si_{s\alpha}(k+1)+T_su_{s\alpha}(k+1) \quad (23)$$

$$\psi_{s\beta}(k+2)=\psi_{s\beta}(k+1)-R_sT_si_{s\beta}(k+1)+T_su_{s\beta}(k+1) \quad (24)$$

$$\begin{aligned} i_{s\alpha}(k+2)=&\frac{R_rT_s}{\delta}\psi_{s\alpha}(k+1)+\frac{L_r\omega_rT_s}{\delta}\psi_{s\beta}(k+1)+\\ &(1-\frac{R_sL_r+R_rL_s}{\delta}T_s)i_{s\alpha}(k+1)-\omega_rT_si_{s\beta}(k+1)\\ &+\frac{L_rT_s}{\delta}u_{s\alpha}(k+1) \end{aligned} \quad (25)$$

$$\begin{aligned} i_{s\beta}(k+2)=&\frac{R_rT_s}{\delta}\psi_{s\beta}(k+1)-\frac{L_r\omega_rT_s}{\delta}\psi_{s\alpha}(k+1)+\\ &(1-\frac{R_sL_r+R_rL_s}{\delta}T_s)i_{s\beta}(k+1)+\omega_rT_si_{s\alpha}(k+1)\\ &+\frac{L_rT_s}{\delta}u_{s\beta}(k+1) \end{aligned} \quad (26)$$

From Eqns. (5) and (6), the predictive values of the stator flux amplitude and electromagnetic torque at the k+2th sampling instant can be obtained as:

$$\begin{cases} \left|\boldsymbol{\psi}_s(k+2)\right| = \sqrt{\psi_{s\alpha}^2(k+2)+\psi_{s\beta}^2(k+2)} \\ T_e(k+2) = \dfrac{3}{2} n_p \boldsymbol{\psi}_s(k+2) \otimes \boldsymbol{i}_s(k+2) \end{cases} \tag{27}$$

The cost functions of the MPDTC with delay compensation and the LSFMPDTC with delay compensation can be expressed as:

$$\begin{aligned} &min.\ J = k_\psi \frac{\left|\boldsymbol{\psi}_s^* - \boldsymbol{\psi}_s^p(k+2)\right|}{\boldsymbol{\psi}_{sN}} + k_T \frac{\left|T_e^* - T_e^p(k+2)\right|}{T_{eN}} \\ &s.t.\quad \boldsymbol{u}_s(k) \in \{\boldsymbol{u}_0, \boldsymbol{u}_1, \ldots, \boldsymbol{u}_6, \boldsymbol{u}_7\} \end{aligned} \tag{28}$$

$$\begin{aligned} &min.\ J = k_\psi \frac{\left|\boldsymbol{\psi}_s^* - \boldsymbol{\psi}_s^p(k+2)\right|}{\boldsymbol{\psi}_{sN}} + k_T \frac{\left|T_e^* - T_e^p(k+2)\right|}{T_{eN}} \\ &\qquad + k_f \sum_{x=a,b,c} \left|S_x(k) - S_x(k-1)\right| \\ &s.t.\quad \boldsymbol{u}_s(k) \in \{\boldsymbol{u}_0, \boldsymbol{u}_1, \ldots, \boldsymbol{u}_6, \boldsymbol{u}_7\} \end{aligned} \tag{29}$$

C. Implementation of the Improved MPDTC Optimization Algorithm

A flowchart of the improved MPDTC optimization algorithm is shown in Fig. 4. It includes the following steps.

Step 1) Measure the current $\boldsymbol{i}_s(k)$, the dc-link voltage $U_{dc}(k)$ and the rotor speed $\omega_r(k)$ at the kth sampling instant.

Step 2) Estimate the stator flux $\hat{\boldsymbol{\psi}}_s(k)$ and rotor flux $\hat{\boldsymbol{\psi}}_r(k)$ at the kth sampling instant using a full order observer.

Step 3) Compensate the time delay by predicting the values of the stator flux $\hat{\boldsymbol{\psi}}_s(k+1)$ and stator current $\hat{\boldsymbol{i}}_s(k+1)$ at the k+1th sampling instant.

Step 4) Calculate the desired voltage vector $\boldsymbol{u}_s^*$ using the stator flux predictive controller. Then calculate the sector of $\boldsymbol{u}_s^*$, and the three voltage vectors in the sector of $\boldsymbol{u}_s^*$ are obtained, which will be evaluated by the cost function.

Step 5) Predict the torque and stator flux for the three voltage vectors, using (27). Then evaluate the cost function J_i using (28) or (29).

Step 6) Find the minimum value of the cost function.

Step 7) Select the optimal voltage vector $\boldsymbol{u}_{opt}(k)$ that minimizes the cost function. Return to Step 1).

V. Simulation Results

To validate the validity of the proposed MPDTC method, a simulation of the proposed MPDTC method was carried out using Matlab/Simulink simulation software. In the MPDTC, the weighting factors k_ψ=2 and k_T=1 have been selected. In the LSFMPDTC, the weighting factors k_ψ=2, k_T=1 and k_f=0.1 have been selected. The PI regulator parameters of the speed loop are K_P=1.2 and K_I=0.35. The current error feedback coefficients of the observer are g_1=−2.8 and g_2=−0.034.

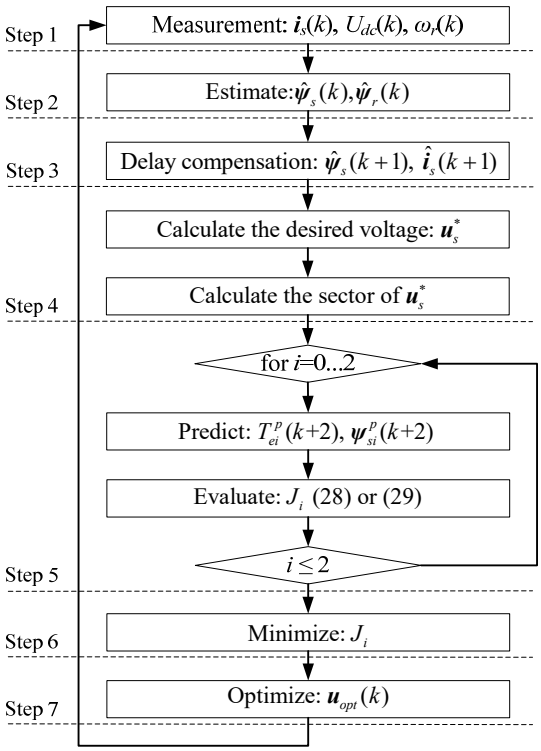

Fig. 4. Flowchart of the improved MPDTC algorithm.

TABLE I
Parameters of the Induction Machine Drive System

Parameters	Value	Parameters	Value
Rated power (kW)	3	Stator resistance (Ω)	1.725
Rated current (A)	6.8	Rotor resistance (Ω)	2.310
Rated voltage (V)	380	Mutual inductance (mH)	228
Rated frequency (Hz)	50	Stator inductance (mH)	240
Rated torque (N·m)	20	Rotor inductance (mH)	240
Rated rotor speed (r/min)	1430	Number of motor pairs	2

The parameters of the induction machine used in the simulation are given in Table I, the sampling frequency is 6kHz and dc-link voltage U_{dc} is 540V.

The dynamic responses of the MPDTC without delay compensation, the MPDTC with delay compensation and the LSFMPDTC with delay compensation are presented in Fig. 5. From top to bottom, the curves shown in Fig. 5 are the stator current, rotor speed, stator flux and electromagnetic torque. The first speed reference is 0-300 r/min at 0.1s, the second speed reference step is from 300 to 600 r/min at 0.8s, and the third speed reference changes is from 600 to 1200 r/min at 1.4s. The first step-up change in the torque reference is from 0 to 10 N·m at 0.4s, and the second torque reference change takes place at 1.2s from 10 to 20 N·m. It can be seen that the torque and current ripples of both the MPDTC with delay compensation and the LSFMPDTC with delay compensation are lower than those of the MPDTC without delay

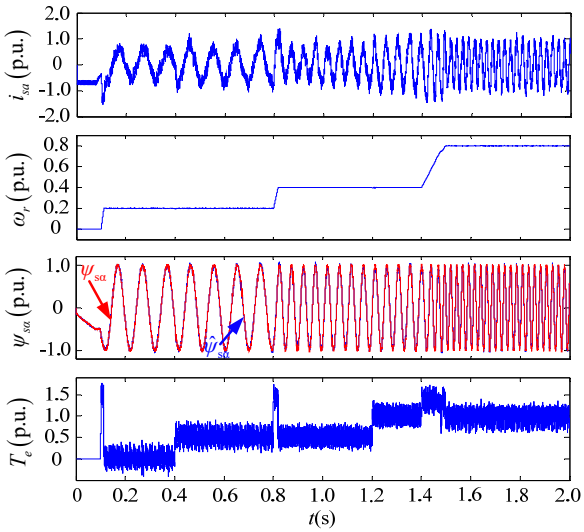

(a) MPDTC without delay compensation.

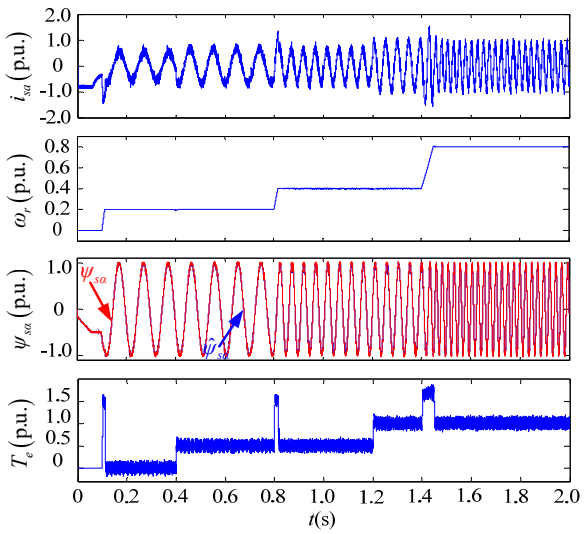

(b) MPDTC with delay compensation.

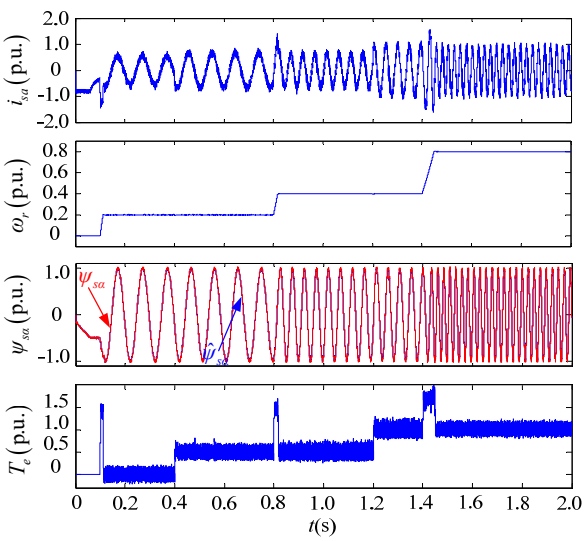

(c) LSFMPDTC with delay compensation.

Fig. 5. Dynamic responses of the stator current, rotor speed, stator flux and electromagnetic torque.

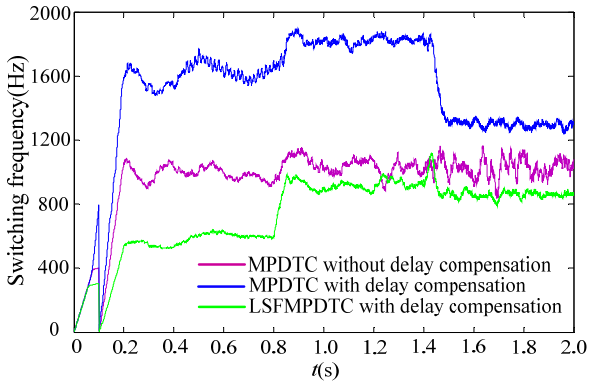

Fig. 6. Average switching frequencies of the three methods.

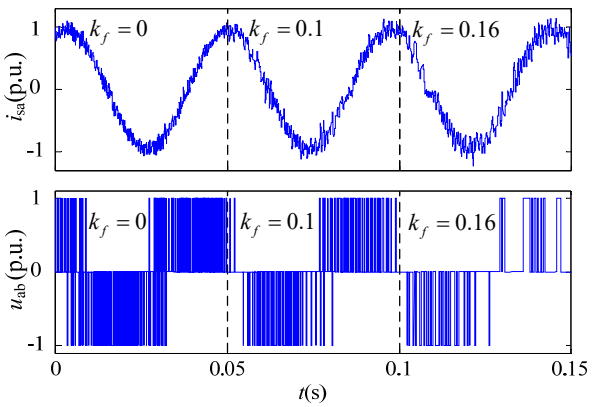

Fig. 7. Simulation results of the current and inverter output voltage under different weighting factors k_f.

compensation. In addition, the steady state performance is significantly improved. This means that the delay compensation can effectively reduce the torque and current ripples. From Fig. 5, it can also be seen that the estimated stator flux $\hat{\psi}_{s\alpha}$ follows the real stator flux $\psi_{s\alpha}$ exactly in both the dynamic state and the steady state.

From the analysis of Fig. 5, it can be seen that the performance of both the MPDTC with delay compensation and the LSFMPDTC with delay compensation are better than that of the MPDTC without delay compensation. However, Fig. 6 shows that the average switching frequency of the MPDTC with delay compensation is higher than that of the MPDTC without delay compensation. The reason for this has already been explained in section Ⅳ-B. When compared to the MPDTC with delay compensation, the LSFMPDTC with delay compensation can significantly reduce the average switching frequency. This indicates that the LSFMPDTC with delay compensation can improve the control performance while minimizing the switching frequency of the inverter.

Under three different weighting factors k_f, the corresponding simulation results of the current i_{sa} and inverter output voltage u_{ab} at 600 r/min with the rated load are presented in Fig. 7. It can be clearly seen that the switching frequency of the inverter is gradually reduced by increasing

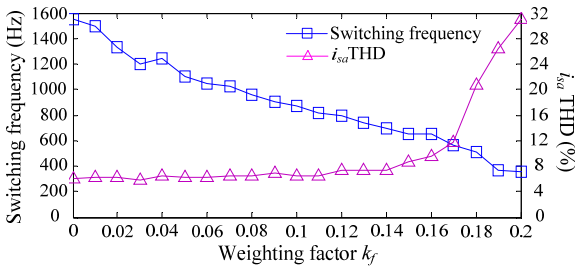

Fig. 8. Influence of the weighting factor on the average switching frequency and current total harmonic distortion.

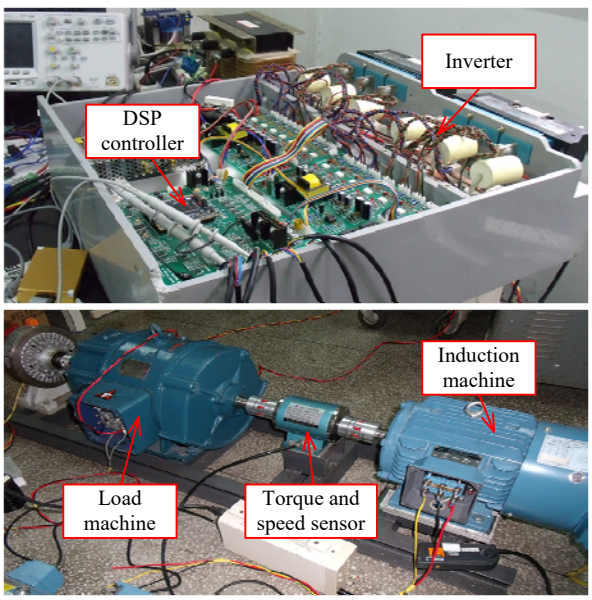

Fig. 9. Experimental platform.

the weighting factor k_f. At the same time, an increasement of k_f leads to a higher current distortion. Fig. 8 shows the influence of different weighting factors k_f on the average switching frequency and current total harmonic distortion. Therefore, the design of the weighting factor k_f is considered to be a trade-off between the switching frequency of the inverter and the current distortion. In both the simulation and experiment, the values of k_ψ , k_T and k_f are adjusted according to the performance of torque, flux and switching frequency. The weighting factor design method needs further research.

VI. Experimental Results

Experimental verification of the proposed control strategy was performed using a TMS320F2812 controller. The experimental platform used in this paper is shown in Fig. 9. The sampling frequency of the control system is set at 6 kHz, and the dc-link voltage is 540V. The parameters of the induction machine are the same as those listed in Table I. The weighting factors k_ψ=3, k_T=1 and k_f=0.14 have been selected. The PI regulator parameters of the speed loop are K_P=2 and K_I=0.2. The current error feedback coefficients of the observer are g_1=−2.8 and g_2=−0.034.

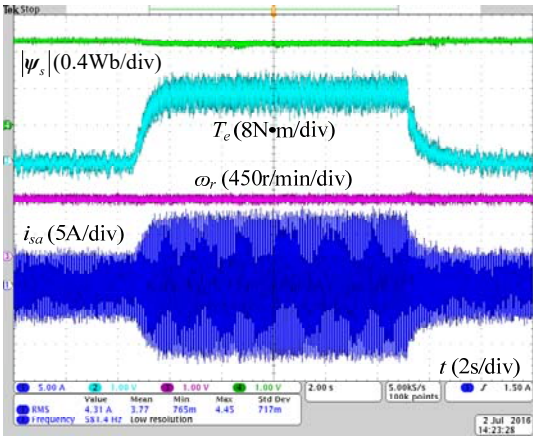

(a) MPDTC without delay compensation.

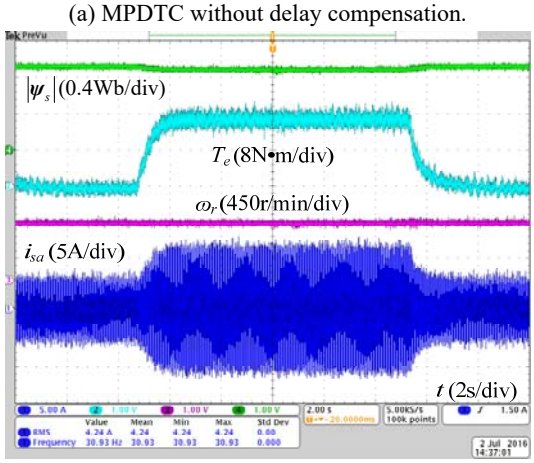

(b) MPDTC with delay compensation.

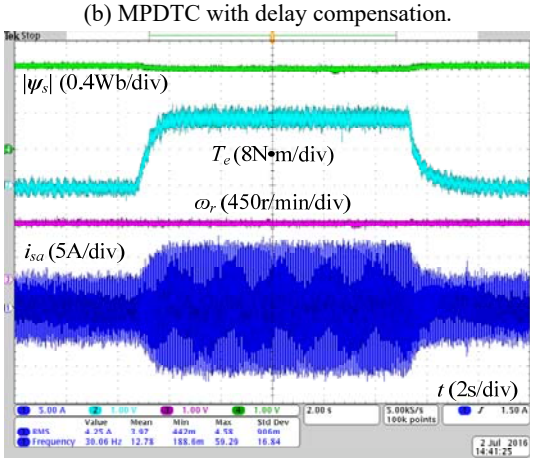

(c) LSFMPDTC with delay compensation.

Fig. 10. Experimental results of three methods under a sudden load disturbance at 900 r/min.

Under an 80% of the rated load disturbance, the stator flux amplitude, torque, rotor speed and stator current waveforms of the MPDTC without delay compensation, the MPDTC with delay compensation and the LSFMPDTC with delay compensation at 900 r/min are shown in Fig. 10. It can be seen that the torque ripples of both the MPDTC with delay compensation and the LSFMPDTC with delay compensation are lower than that of the MPDTC without delay compensation. The stator flux amplitude waveforms of

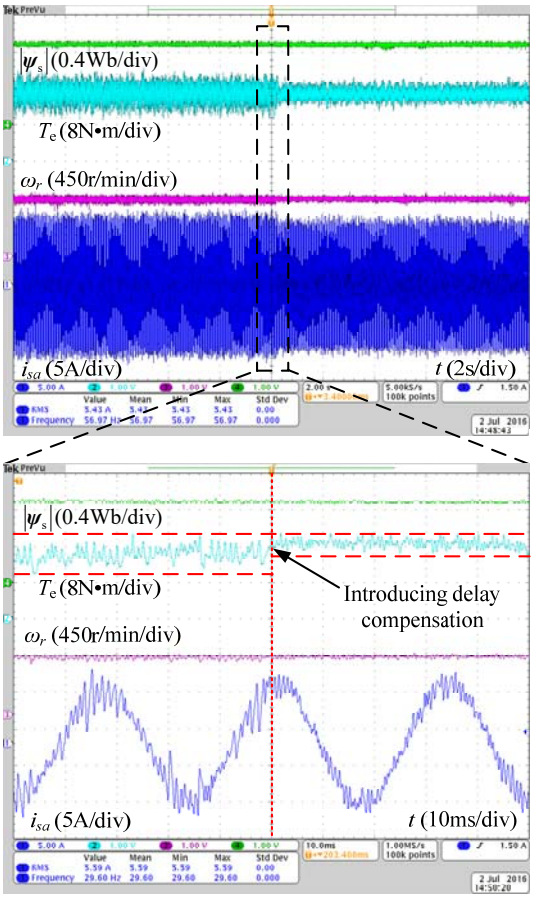

Fig. 11. Experimental result comparison between the MPDTC without delay compensation and the MPDTC with delay compensation at 900 r/min.

the three methods have a slight drop, and the rotor speed responses of the three methods are almost unchanged.

A performance comparison between the MPDTC without delay compensation and the MPDTC with delay compensation at 900 r/min with 80% of rated load is presented in Fig. 11. The left half of Fig. 11 shows experimental results of the MPDTC without delay compensation, and the right half of Fig. 11 shows experimental results of the MPDTC with delay compensation. It is clearly seen that the current and torque ripples of the MPDTC with delay compensation are lower than those of the MPDTC without delay compensation.

Under a 50% of the rated load disturbance, experimental results of the LSFMPDTC with delay compensation at 300 r/min are shown in Fig. 12 (a), and the steady state experimental results are given in Fig. 12 (b). It can be observed that the stator flux amplitude and rotor speed are almost unchanged under the 50% of the rated load disturbance. The performance of the torque and stator current are good in the steady state.

The computation times of both the conventional MPDTC and the improved MPDTC operating with or without delay compensation are shown in Fig. 13. In either case, it can

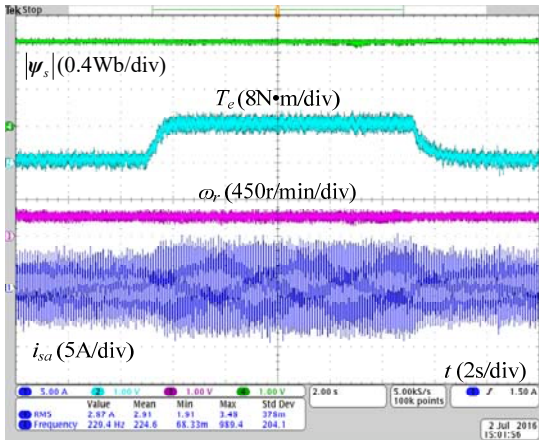

(a) Under a 50% of the rated load disturbance.

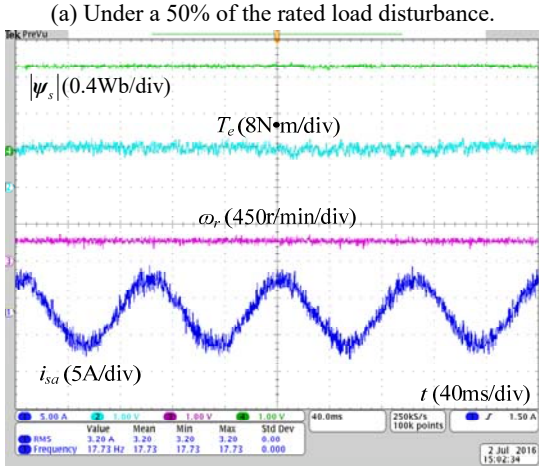

(b) Steady state operation.

Fig. 12. Experimental results of the LSFMPDTC with delay compensation at 300 r/min.

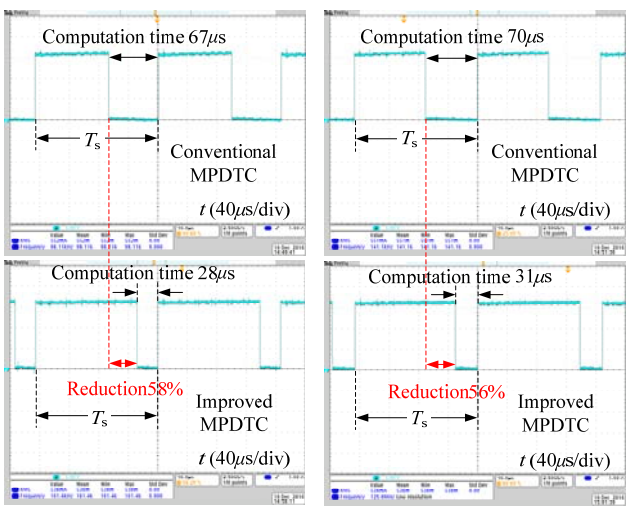

(a) Without delay compensation. (b) With delay compensation.

Fig. 13. Comparison of the computation time between the conventional MPDTC and the improved MPDTC.

be clearly seen that the improved MPDTC is able to reduce the computation time by more than 50% when compared with the conventional MPDTC. This means that the improved MPDTC has better computing performance.

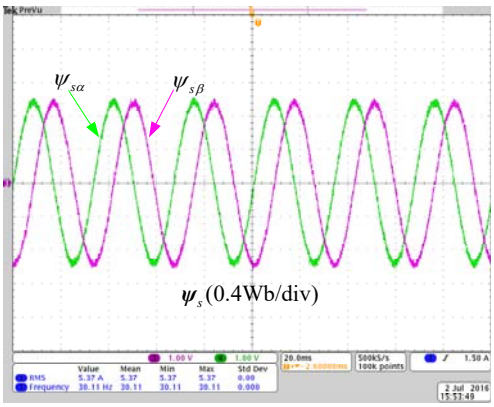

(a) Stator flux.

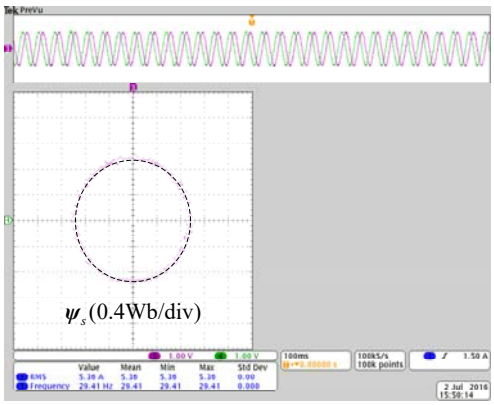

(b) Stator flux locus.

Fig. 14. Stator flux waveforms of the LSFMPDTC with delay compensation at 900 r/min.

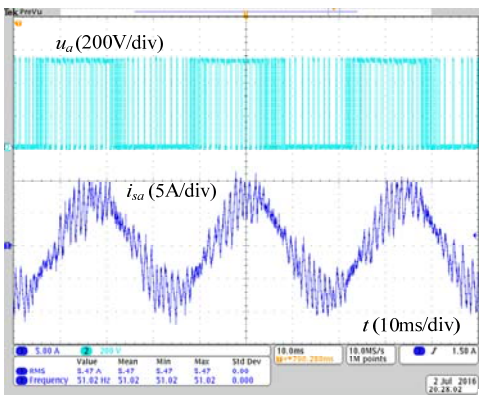

(a) MPDTC without delay compensation.

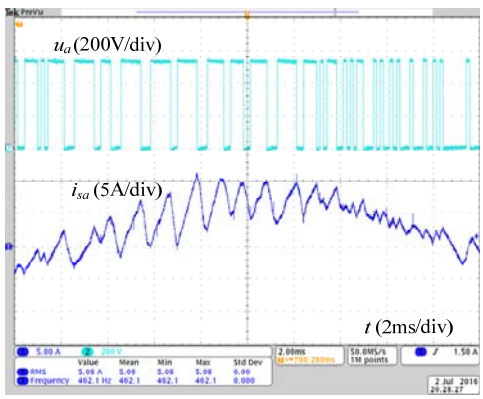

(b) Zoom-in view of the MPDTC without delay compensation.

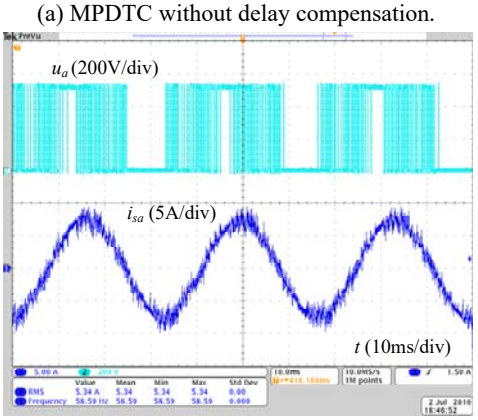

(c) MPDTC with delay compensation.

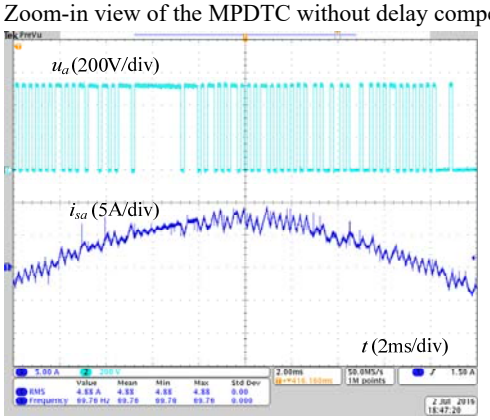

(d) Zoom-in view of the MPDTC with delay compensation.

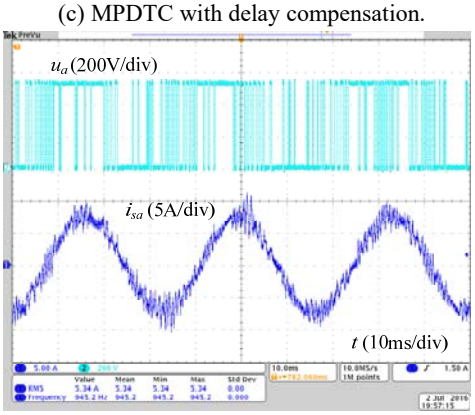

(e) LSFMPDTC with delay compensation.

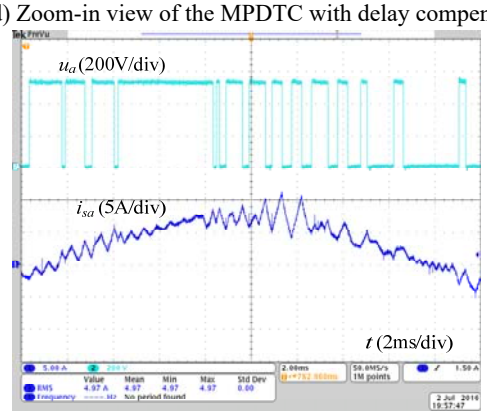

(f) Zoom-in view of the LSFMPDTC with delay compensation.

Fig. 15. Experimental results of the current i_{sa} and inverter output voltage u_a at 900 r/min with 80% of the rated load.

The stator flux responses of the LSFMPDTC with delay compensation at 900 r/min with 80% of the rated load are depicted in Fig. 14. Fig. 14(a) shows that the waveforms of the stator flux $\alpha\beta$ frame components are very smooth. From Fig. 14(b), it can be observed that the stator flux locus can follow the circle.

Experimental results of the current i_{sa} and inverter output voltage u_a at 900 r/min with 80% of the rated load are described in Fig. 15. This clearly indicates that the average switching frequency of the MPDTC with delay compensation is higher than that of both the MPDTC without delay compensation and the LSFMPDTC with delay compensation. Via counting the number of switchings in a period of time, the average switching frequency of the MPDTC without delay compensation, the MPDTC with delay compensation and the LSFMPDTC with delay compensation are obtained. They are 1.1 kHz, 1.8 kHz and 1kHz, respectively.

VII. CONCLUSIONS

This paper has proposed an improved MPDTC method for induction machine drives. The three voltage vectors evaluated by the cost function have been obtained by a stator flux predictive controller. Therefore, the computational burden of the conventional MPDTC has been effectively reduced. The advantages of the improved MPDTC method become more obvious, if a system utilizes a multilevel (e.g., three-level, five-level) converter. Delay compensation has been adopted for the effect of time delay in this paper. The current and torque ripples caused by the time delay are significantly reduced. Furthermore, by introducing a constraint on the power semiconductors switching number to the cost function of the MPDTC, the LSFMPDTC method has been developed. The switching frequency of the inverter can be reduced by increasing the weighting factor k_f of the switching frequency. However, the current distortion is increased at the same time. Both simulation and experimental results have shown that the stator flux obtained from the full order observer can follow the real stator flux exactly. The improved MPDTC method has good dynamic and steady state performance and can significantly reduce the switching frequency.

ACKNOWLEDGMENT

This work was supported in part by grant from the National Natural Science Foundation of China under project 51377102.

REFERENCES

[1] R. Datta and V. T. Ranganathan, "A simple position-sensorless algorithm for rotor-side field-oriented control of wound-rotor induction machine," *IEEE Trans. Ind. Electron*., Vol.48, No.4, pp. 786-793, Aug. 2001.

[2] I. Takahashi and T. Noguchi, "A new quick-response and high-efficiency control strategy of an induction motor," *IEEE Trans. Ind. Appl*., Vol. IA-22, No. 5, pp. 820-827, Sep. 1986.

[3] C. Lascu, I. Boldea, and F. Blaabjerg, "A modified direct torque control for induction motor sensorless drive," *IEEE Trans. Ind. Appl.*, Vol. 36, No. 1, pp. 122-130, Jan. 2000.

[4] D. Casadei, F. Profumo, G. Serra, and A. Tani, "FOC and DTC: two viable schemes for induction motors torque control," *IEEE Trans. Power Electron.*, Vol. 17, No. 5, pp. 779-787, Sep. 2002.

[5] Z. Sorchini and P. T. Krein, "Formal derivation of direct torque control for induction machines," *IEEE Trans. Power Electron.*, Vol. 21, No. 5, pp. 1428-1436, Sep. 2006.

[6] N. R. N. Idris, C. L. Toh and M. E. Elbuluk, "A new torque and flux controller for direct torque control of induction machines," *IEEE Trans. Ind. Appl*., Vol. 42, No. 6, pp. 1358-1366, Nov. 2006.

[7] X. Qiu, W. X. Huang and F. F. Bu, "Torque-angle-based direct torque control for interior permanent-magnet synchronous motor drivers in electric vehicles," *Journal of Power Electronics*, Vol. 13, No. 6, pp. 964-974, Nov. 2013.

[8] S. Arumugam and M. Thathan, "Novel switching table for direct torque controlled permanent magnet synchronous motors to reduce torque ripple," *Journal of Power Electronics*, Vol. 13, No. 6, pp. 939-954, Nov. 2013.

[9] A. Jidin, N. R. N. Idris, A. H. M. Yatim, T. Sutikno, and M. E. Elbuluk, "Extending switching frequency for torque ripple reduction utilizing a constant frequency torque controller in DTC of induction motors," *Journal of Power Electronics*, Vol. 11, No. 2, pp. 148-155, Mar. 2011.

[10] H. F. Rashag, S. P. Koh, A. N. Abdalla, N. M. L. Tan, and K. H. Chong, "Modified direct torque control using algorithm control of stator flux estimation and space vector modulation based on fuzzy logic control for achieving high performance from induction motors," *Journal of Power Electronics*, Vol. 13, No. 3, pp. 369-380, May 2013.

[11] S. Kouro, P. Cortés, R. Vargas, U. Ammann, and J. Rodriguez, "Model predictive control – A simple and powerful method to control power converters," *IEEE Trans. Ind. Electron*., Vol. 56, No. 6, pp. 1826-1838, May 2009.

[12] L. Tarisciotti, G. L. Calzo, A. Gaeta, P. Zanchetta, F. Valencia, and D. Saez, "A distributed model predictive control strategy for back-to-back converters," *IEEE Trans. Ind. Electron*., Vol. PP, Feb. 2016.

[13] J. Rodriguez, R. M. Kennel, J. R. Espinoza, M. Trincado, C. A. Silva, and C. A. Rojas, "High-performance control strategies for electrical drives: An experimental assessment," *IEEE Trans. Ind. Electron*., Vol. 59, No. 2, pp. 812-820, May. 2012.

[14] J. Holtz and S. Stadtfeld, "A predictive controller for the stator current vector of AC-machines fed from a switched voltage source," *Int. Power Electron. Conf.*, Vol. 2, pp. 1665–1675, Mar. 1983.

[15] W. Xie, X. Wang, F. Wang, W. Xu, R. M. Kennek, D. Gerling, and R. D. Lorenz, "Finite control set-model predictive torque control with a deadbeat solution for PMSM drives," *IEEE Trans. Ind. Electron*., Vol. 62, No. 9, pp. 5402-5410,Sep. 2015.

[16] S. Kwak and J. C. Park, "Switching strategy based on model predictive control of VSI to obtain high efficiency and balanced loss distribution," *IEEE Trans. Power Electron*., Vol. 29, No. 9, pp. 4551-4567,Sep. 2014.

[17] F. Villarroel, J. R. Espinoza, C. A. Rojas, J. Rodriguez, M. Rivera, and D. Sbarbaro, "Multiobjective switching state selector for finite-states model predictive control based on fuzzy decision making in a matrix converter," *IEEE Trans.*

Ind. *Electron*., Vol. 60, No. 2, pp.589-599,Feb. 2013.
[18] C. S. Lim, N. A. Rahim, W. P. Hew, and E. Levi, "Model predictive control of a two-motor drive with five-leg-inverter supply," *IEEE Trans*. *Ind. Electron*., Vol. 60, No. 1, pp. 54-65, Jan. 2013.
[19] J. Rodriguez, J. Pontt, C. A. Silva, P. Correa, P. Lezana, P. Cortes, and U. Ammann, "Predictive current control of a voltage source inverter," *IEEE Trans*. *Ind*. *Electron*., Vol. 54, No. 1, pp. 495-503, Feb. 2007.
[20] P. Karamanakos, P. Stolze, R. Kennel, S. Manias, and T. Mouton, "Variable switching point predictive torque control," in *Proc. IEEE Int*. *Conf*. *Ind*. *Technol*., Cape Town, South Africa, pp. 422–427, Feb. 2013.
[21] Y. Zhang, J. Zhu, Z. Zhao, W. Xu, and D. G. Dorrell, "An improved direct torque control for three-level inverter-fed induction motor sensorless drive," *IEEE Trans*. *Power Electron*., Vol. 27, No. 3, pp.1502-1513, Mar. 2012.

Wenxiang Song was born in Jiangsu, China, in 1973. He received his B.S. and M.S. degrees in Electrical Engineering from the China University of Mining and Technology, Xuzhou, China, in 1995 and 1998, respectively; and his Ph.D. degree in Electrical Engineering from the School of Mechatronic Engineering and Automation, Shanghai University, Shanghai, China, in 2006. From September 2006 to December 2008, he was a Post-doctoral Scholar at Shanghai Jiaotong University, Shanghai, China. From 1998 to 2002, he was with Dongfang Electronics, Yantai, China. In 2009, he joined Shanghai University as an Associate Professor in the School of Mechatronic Engineering and Automation, where he has been a Professor since 2015. His current research interests include AC motor control, power electronic converters, and PWM converter/inverter systems.

Shengkang Le was born in Jiangxi, China, in 1990. He received his B.S. degree in Automation from Shanghai University, Shanghai, China, in 2014. He is presently a graduate student at Shanghai University. His current research interests include model predictive control, power electronics, and high-performance induction machine control systems.

Xiaoxin Wu was born in Jiangsu, China, in 1978. He received his B.S. degree in Electronics Engineering from the Nanjing University of Aeronautics and Astronautics, Jiangsu, China, in 2000; and his M.S. degree in the School of Mechatronic Engineering and Automation from Shanghai University, Shanghai, China, in 2006. From 2006 to 2010, he was working as a Lecturer in the Department of Electrical Engineering of Nantong University, Nantong, China, where he has been an Associate Professor since 2011. His current research interests include AC motor control, DC-DC converters, and PWM converter/inverter systems.

Yi Ruan was born in Shanghai, China, in 1955. He received his B.S. degree from Tongji University, Shanghai, China, in 1984; his M.S. degree from the Shanghai University of Technology, Shanghai, China, in 1989; and his Ph.D. degree from Shanghai University, Shanghai, China, in 1996. In 1989, he joined Shanghai University, where he was promoted to Professor in 2003. He was a visiting faculty member at Brunswick University of Technology, Braunschweig, Germany, from 1993 to 1994. His current research interests include control strategies of electrical drive systems, modern control theory and its application to electrical drive systems, and the application of power electronics in renewable energy systems.